OXFORD UNIVERSITY PRESS | The Journal of Geophysics and Engineering

A COMPARISON OF METHODS FOR ESTIMATING Q

Journal:	*The Journal of Geophysics and Engineering*
Manuscript ID	JGE-2018-0110
Manuscript Type:	Paper
Date Submitted by the Author:	01-Sep-2018
Complete List of Authors:	Lei, Xiong; Pennsylvania State University, Energy and Mineral Engineering Morgan, Eugene; Pennsylvania State University, Energy and Mineral Engineering
Keywords:	quality factor, seismic attenuation, attenuation estimation, window size, "thin-layer" effect, effective bandwidth coefficient

IOP Publishing Journal of Geophysics and Engineering
Journal **XX** (XXXX) XXXXXX https://doi.org/XXXX/XXXX

A COMPARISON OF METHODS FOR ESTIMATING *Q*

Xiong Lei and Eugene Morgan

Department of Energy and Mineral Engineering, Pennsylvania State University, State College, USA

E-mail: xiong.lei@outlook.com

Received xxxxxx
Accepted for publication xxxxxx
Published xxxxxx

Abstract

As a quantitative measure of seismic attenuation, quality factor (*Q*) is useful to directly indicate hydrocarbon, assist inverse *Q* filtering, and forward model seismic wave propagation; however, quality factor remains difficult to reliably measure from seismic data. Many approaches in either the time or frequency domain have been proposed in the past. Among them, the most popular approaches are the spectral ratio method, centroid frequency shift method, and peak frequency shift method. They are the base of many newly proposed methods and a lot of case studies had implemented them to estimate *Q*, but no benchmarking of these methods currently exists giving an objective comparison of their performances. Furthermore, little guidance is given to the practitioner on how best to implement these methods, namely: is there a best way to utilize those methods in order to more accurately extract *Q*? In this paper, we performed a detailed analysis and comparison of those methods on synthetic seismic data with specified *Q* values. We applied the three methods under different preprocessing techniques, frequency bandwidths, signal frequencies, signal-to-noise ratios (S/N), and *Q* models. We find that *Q* is estimated most accurately under the following conditions: a) using the centroid frequency shift or spectral ratio methods after running FFT on windowed seismic amplitudes or running FFT on extracted wavelets; b) truncating the frequency bandwidth with coefficients between 0.2 ~ 0.4; c) data with higher frequency; d) data with less noise; and e) dealing with layers with lower *Q* (higher attenuation).

Keywords: quality factor, seismic attenuation, attenuation estimation, window size, "thin-layer" effect, effective bandwidth coefficient

1. Introduction

In seismic interpretation, *Q* is an important geophysical attribute of the subsurface. It is associated with the intrinsic physical properties of rocks and fluids (Winkler and Nur 1982; Sheriff and Geldart 1995), as well as the scattering effect of the seismic wave (Goutbeek *et al* 2004); thus, *Q* can be partitioned into two major factors: 1) intrinsically anelastic energy loss due to viscous effect of the pore fluids, shearing at grain boundaries, and mineral dislocations, and 2) scattering energy loss due to the spherical spreading of the wavefront and diffraction at heterogeneities (Hatzidimitriou 1994; Goutbeek *et al* 2004, Müller *et al* 2010). The difference between these two mechanisms lies in the factor that the energy of the former one is transferred into heat which is unconservative, while the later one mainly results from the geometrical energy redistribution (Gao *et al* 1998, Hatzidimitriou 1994). Since the intrinsic *Q*, due to the first mechanism, is related to the physical properties of rocks and fluids (Winkler and Nur 1982, Sheriff and Geldart 1995), it is a valuable diagnostic tool for reservoir characterization and hydrocarbon detection (Toksöz *et al* 1979, Frisillo and Stewart 1980). Additionally, the intrinsic *Q* is crucial to interpret the effect of AVO, improve the resolution of seismic imaging, and advance the study of material properties. However, intrinsic *Q* remains a difficult seismic attribute to measure from field data,

and few guidelines exist that speak to the reliability of methods for estimating Q.

Currently, many methods exist to estimate quality factor from seismic transmission data such as VSP (e.g., Hauge 1981) and crosswell (e.g., Quan and Harris 1997, Neep *et al* 1996), or seismic reflection data such as CDP gathers (e.g., Jannsen *et al* 1985, Tonn 1991) and CMP gathers (e.g., Dasgupta and Clark 1998, Hackert and Parra 2004). These methods operate in either the time domain or frequency domain. For time-domain approaches, the simplest one is the amplitude decay method, which is directly derived from the quality factor definition. It quantitively calculates the maximum amplitude reduction, thus has a high requirement of the amplitude conservation. In 1974, Gladwin and Stacey put forward that the quality factor could be determined by risetime, defined as the time from the intersection of the steepest rise of a wavelet to its peak wavelet amplitude. This empirical method is insensitive against secondary arrivals. Kjartansson (1979) compensated for the lack of theoretical background of the risetime approach. The wavelet modeling method (Jannsen *et al* 1985) is an optimization procedure that matches a reference signal with the observed signal. One main problem of this method is its low tolerance of the ambient noise, spherical spreading, or scattering effect. In 1996, Engelhard derived an expression for the seismic quality factor with instantaneous amplitude and frequency of seismic traces, known as the analytical signal method. It considers geometrical spreading, but time synchronization is a difficult issue to tackle. More recently, an accurate time-domain method was the matching filter method (Cheng and Margrave 2013). It is a time-domain alternative to spectrum modeling methods (Jannsen *et al* 1985, Tonn 1991, Blias 2011) and very robust to cope with noise on reflection data.

However, the frequency domain methods perform better than those in the time domain, mainly because Q factor almost exclusively has an effect on the shape of the spectrum while the seismic amplitude might be affected by many factors such as underground structure, geometric spreading, and automatic gain control. It is easier to separate the intrinsic attenuation from frequency-independent factors such as spherical spreading or reflectivity (Tu and Lu 2010) in the spectral domain. For the purpose of the attenuation measurement, the process of wave propagation is assumed to be a linear system. If the spectrum of the seismic source wavelet is $S(f)$, the absorption response is $H(f)$, geometrical spreading and transmission responses are included in $G(f)$, and the received amplitude spectrum is $R(f)$. The spectral ratio method (SRM) (Bath 1974, Hauge 1981) obtains relatively accurate Q measurements from the logarithmic ratio of the amplitude spectra assuming that the spherical spreading and scattering is frequency-independent; thus, we have the following expression (Bath 1974, Hauge 1981)

$$H(f) = e^{-\frac{\pi f t}{Q}}, \tag{1}$$

$$ln\left(\frac{R(f)}{S(f)}\right) = -\frac{\pi t}{Q} f + lnG. \tag{2}$$

So, Q is related to the slope of a line fitted to the logarithmic ratio (as Figure 1). This method has been commonly used in practice. Please note that the estimated Q is sensitive to spectral notching and the choice of the effective frequency bandwidth (Tu and Lu 2010). Pinson *et al* (2008) applied an interactively reweighted robust least-squares regression to suppress outliers caused by noise. However, how to choose a proper effective frequency bandwidth is essential and still needs further investigation.

In 1984, Raikes and White employed the idea of matching at different stages of estimation procedures and proposed a matching technique method. Its expression is almost the same as spectral ratio method except for an additional constant and ratio of a transfer function. Another spectral method is spectrum modeling method, which is a byproduct of the wavelet modeling method (Jannsen *et al* 1985, Tonn 1991) and a frequency-domain alternative to the matching filter method (Cheng and Margrave 2013). It does not need the assumption that reflection coefficient and phase velocity are independent of frequency.

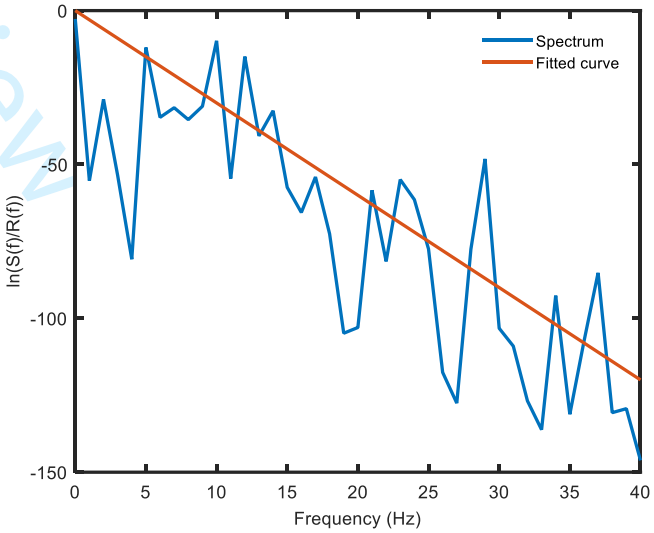

Figure 1 Schematic diagram for the spectral ratio method.

Instead of using the spectral ratio, Quan and Harris (1997) presented a centroid frequency shift method (CFS) to estimate Q in heterogeneous media. As other spectral approaches, it has a strong capability of resisting frequency-independent noise. Quan and Harris (1997) proposed, if the incident spectrum $S(f)$ is Gaussian, and reflected spectrum is denoted by $R(f)$, the quality factor is as follows

$$Q = \frac{\pi(t_r - t_s)\sigma^2}{f_s - f_r} \tag{3}$$

where the centroid frequencies f_s, f_r and spectral variance σ^2 are defined by (as Figure 2)

$$f_s = \frac{\int f|S(f)|df}{\int |S(f)|df}, \tag{4}$$

$$f_r = \frac{\int f|R(f)|df}{\int |R(f)|df}, \tag{5}$$

$$\sigma_s^2 = \frac{\int (f - f_s)^2|S(f)|df}{\int |S(f)|df}. \tag{6}$$

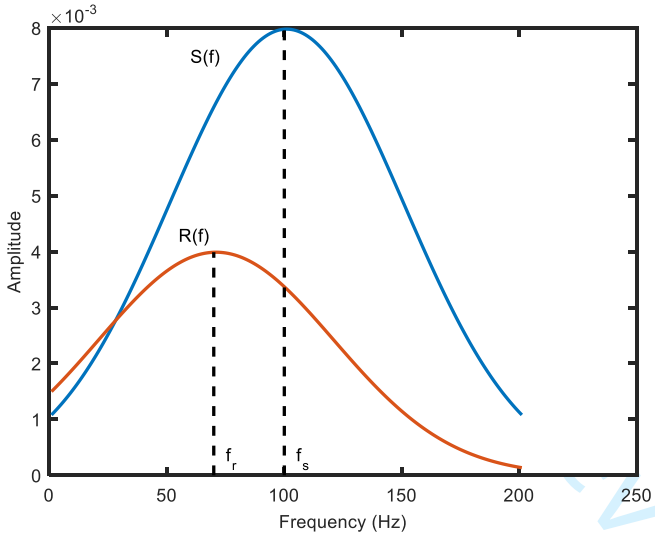

Figure 2 Schematic diagram of the centroid frequency shift method.

The methods above are all for poststack or zero-offset data. For CMP gathers, Dasgupta and Clark (1998) proposed a *Q*-versus-offset (QVO) method. They applied the classical SRM trace by trace and took the average *Q*. Hackert and Parra (2004) improved the QVO method to remove the tuning effect by using well-log-based localized spectral correction. One of the latest methods for CMP gathers is the peak frequency shift method (PFS) (Zhang and Ulrych 2002). PFS calculates *Q* from the reduction of peak frequencies f_p at different offsets. *Q* is expressed in terms of the f_p of the reflection waveform and the dominant frequency f_m of the source wavelet that is assumed to be a Ricker wavelet (as Figure 3).

$$Q = \frac{\pi t f_p f_m^2}{2\left(f_m^2 - f_p^2\right)}. \tag{7}$$

This method is compatible with both CMP gathers and poststack data.

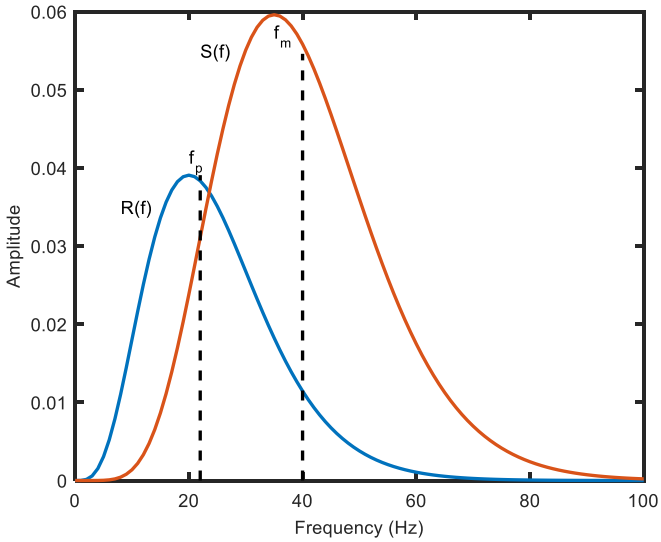

Figure 3 Schematic diagram of the peak frequency shift method.

More advanced methods based on them are proposed afterwards. For example, CFS was initially developed to conduct the attenuation tomography in Quan and Harris's paper (1997). In 2016, Dutta and Schuster optimized the difference between the observed peak frequency shift and the predicted one to realize a wave-equation *Q* tomography. However, there are still risks of *Q* tomography, which lie in the error propagation from the velocity values to the *Q* values. The tomography technique heavily relies on the velocity model, most likely resulting in the slow or even no convergence problem for noise-rich data or data with a less accurate velocity model (Rossi *et al* 2007). Moreover, most of them are developed specially for earthquake records, of which the energy source or reference trace is easily set. Nevertheless, when it comes to engineering projects, the effective energy of the source is difficulty to determine. So, the spectral methods in estimating *Q* are so important as to be worthy of devoting efforts on analyzing or improving the current ones. The current spectral methods also have some limitations in practical applications. For instance, CFS has the assumption that attenuation is linearly proportional to the frequency, meaning the *Q* is independent of frequency; PFS assumes a Ricker wavelet as the source when deriving the *Q* estimation equations, which is hardly satisfied in practice. Moreover, most applications of attenuation estimation used cross-well data or head waves. But seismic reflection data is handier and more desired to be effectively used. Accurately estimating *Q* from reflection data necessitates some special data-preprocessing techniques which try to satisfy those assumptions before conducting estimation (Tu and Lu 2010). However, the specific techniques to cope with the corresponding issues, comparison of the efficacy for different approaches, and a clear recommendation on which methods are the best to use under which circumstances are rarely saw.

It is expected to have one which would facilitate the practical application of spectral methods or the advanced Q tomography.

In this paper, we are committed to compare popular intrinsic Q measurements, particularly focusing on the frequency-domain methods: spectral ratio method, centroid frequency shift method, and peak frequency shift method. These popular methods have shown greater success in the literature than other methods (e.g., Sams and Goldberg 1990, Rickett 2006, Tu and Lu 2010, Tary *et al* 2017, Oliveira *et al* 2017, Zhang *et al* 2016); however, we do not expect a method that would work perfectly under any condition (Tonn 1991). Here, we focus on the investigation of the performance of those three popular methods, figuring out the proper one for a specific condition and suggesting optimal preprocessing techniques. In terms of extracting Q from reflection data, this paper discusses five data-preprocessing techniques that help to improve the quality of frequency-domain data and conserve more useful information. Subsequently, we evaluate the performance of various combinations of techniques and methods using synthetic seismic reflection data. We also test them on models with different Q's, different S/Ns, different frequencies, and different effective frequency bandwidths. The goal of this study is to comprehensively diagnose these methods under varieties of model conditions with various preprocessing techniques and to ultimately provide insights on the optimal choices of preprocessing techniques and estimation methods for a given model, deeply understanding the impact factors of Q measurements.

2. Methodology

Different kinds of noise caused by the ambient condition, equipment, or personal error would distort the time or frequency characteristics of the signal, affecting the accuracy of Q estimation. The demand for noise suppression necessitates data preprocessing. The techniques such as time-frequency transformation, window functions, zero padding, and so forth would be discussed below. Meanwhile, excessive processing would cut down the reliability of estimation since the conservation of the useful information would also be impaired somehow by processing techniques. The degree of preprocessing, such as how much band-pass filter, what kind of window function, what kind of time-frequency decomposition techniques, or, especially, which effective frequency bandwidth (Figure 4), is worth researching.

In particular, the frequency-based methods largely depend on the quality of the time-frequency decomposition. The conventional Fast Fourier Transform (FFT) suffers from the trade-off in time localization and spectral resolution, where a smaller window size will be more representative of the target interface, but its spectrum will be more band limited. Using a continuous wavelet transform (CWT) instead of FFT affords better time localization without the subjectivity of the window choice. However, this comes at the cost of subjectivity in the choice of mother wavelets to use as the basis of the transformation. One would want this mother wavelet to resemble the source wavelet. But in practice, the source wavelet may be unknown. In this section, we offered five candidate preprocessing workflows that focus on exploring the impact of CWT over FFT, as well as other techniques stated before.

2.1 Technique I

Firstly, in case of frequency leakage, the Hamming window is a good choice to taper the target signal for spectral transformation. It keeps the high level of frequency resolution and is easily implemented (Harris 1978). Then, the time series corresponding to each window is transformed into the frequency domain via FFT after zero-padding, which improves the spectral resolution. Sometimes, residual noise in signals would largely impair the spectra. In order to further mitigate the residual noise, a moving average filter is a common technique to smooth the spectra (Karl 1989). A crucial factor impacting the accuracy of Q estimation is the effective frequency bandwidth, which suppresses the very lower and very higher frequency noise. Tu and Lu (2010) suggested determining the bandwidth by an effective-bandwidth coefficient ε (Figure 4).

$$f_{eff} \in \{R(f) \geq \varepsilon \cdot max(|R(f)|)\} \tag{8}$$

where $R(f)$ is the received wavelet spectrum. The effective bandwidth f_{eff} is defined as frequencies when the amplitudes are less than a threshold that is adjusted by ε. The smaller the coefficient, the wider the frequency bandwidth. Subsequently, both the effective received wavelet $R(f)$ and effective source wavelet $S(f)$ are determined by the newly defined bandwidth. At the end, the well-prepared data is used to measure the Q. These steps are displayed conceptually in Figure 5.

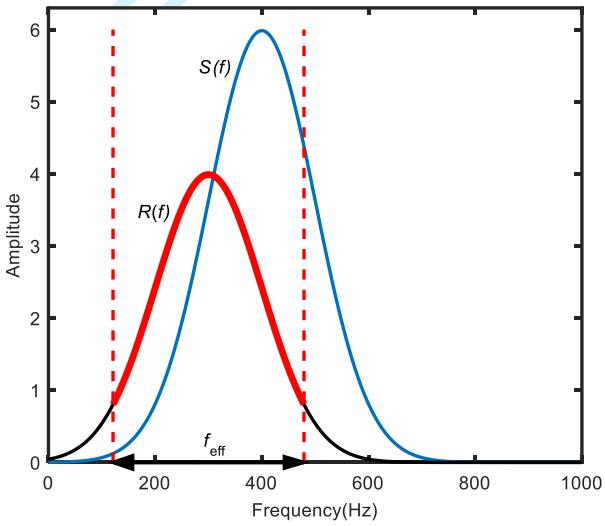

Figure 4. Definition of effective frequency bandwidth.

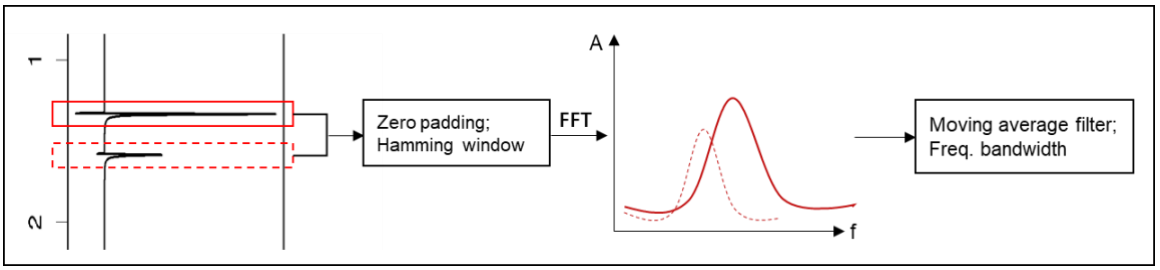

Figure 5. Schematic diagram of technique I.

2.2 Technique II

The target reflection data is transformed into the time-frequency domain through the CWT with a Morlet mother wavelet, of which the central frequency f_c = 0.1 Hz and the standard deviation of its Gaussian envelope σ = 5 (Figure 6). Q would be estimated by methods discussed above based on the time slices of the scalogram for source and reflection interfaces. Again, the moving average filtering and the frequency bandwidth constraint are imposed on the spectrum before Q estimation.

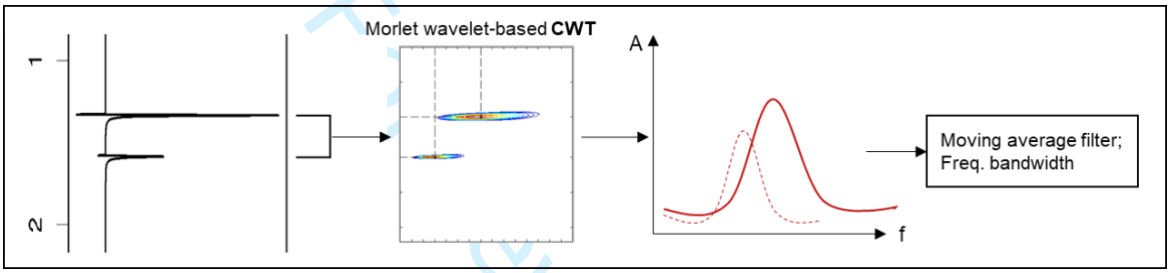

Figure 6. Schematic diagram of technique II.

2.3 Technique III

Here, we apply the same steps to preprocess the data as in Technique II, except that the assumed Morlet wavelet is replaced by a statistically extracted wavelet. Specifically speaking, when analyzing the time-frequency spectrum via continuous wavelet transformation, the mother wavelet is extracted by the technique of Lu *et al* (2007) on the target windowed data, instead of the default Morlet wavelet (Figure 7). His method assumes the wavelet fourth-order moment is approximately equal to the fourth-order cumulant of the seismic data. Subsequently, the wavelet is iteratively solved by minimizing the cost function. Comparing Figure 6 and Figure 7, the operational difference between Techniques II and III lies in the mother wavelet choice.

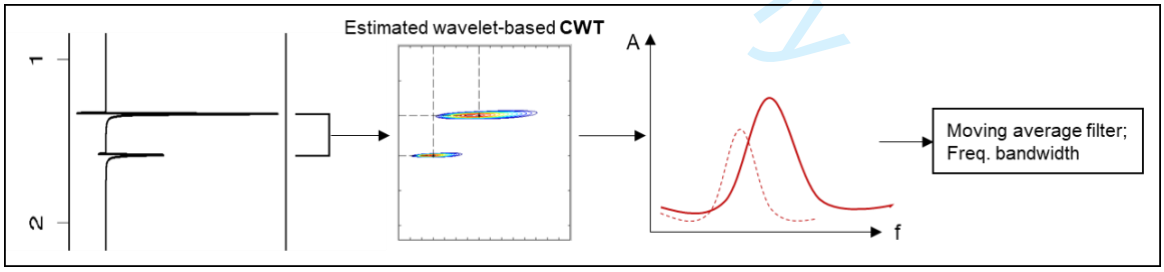

Figure 7. Schematic diagram of technique III.

2.4 Technique IV

After denoising, here we estimate wavelets from both truncated source and reflection signals by Lu's method. Then, we conduct FFT to transform the estimated wavelets from the time domain to frequency domain. Before FFT, the Hamming window and zero padding technique are also implemented on the wavelet (Figure 8). Now, those two wavelets represent the source and reflected waves. Then the moving average filter smooths their spectra before Q estimation. This process is approximately identical to that proposed by Tu and Lu (2010), except that he used a reflectivity sequence to calibrate the spectrum.

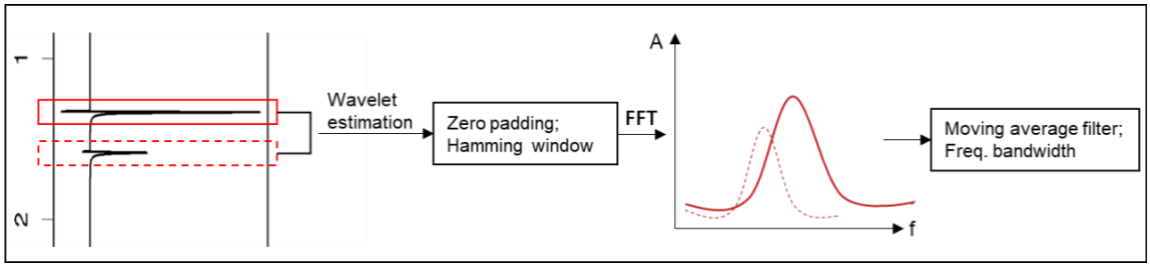

Figure 8. Schematic diagram of technique IV.

2.5 Technique V

As illustrated in Figure 9, the last approach carries out the CWT with a Morlet mother wavelet on the new wavelets which are estimated by Lu's method from source and reflection signals, respectively. The parameters of Morlet mother wavelet are the same as that in Technique II. This differs from Technique II in that here the CWT is being performed on the extracted wavelets representing the source and reflected waves, instead of directly running CWT on the signals.

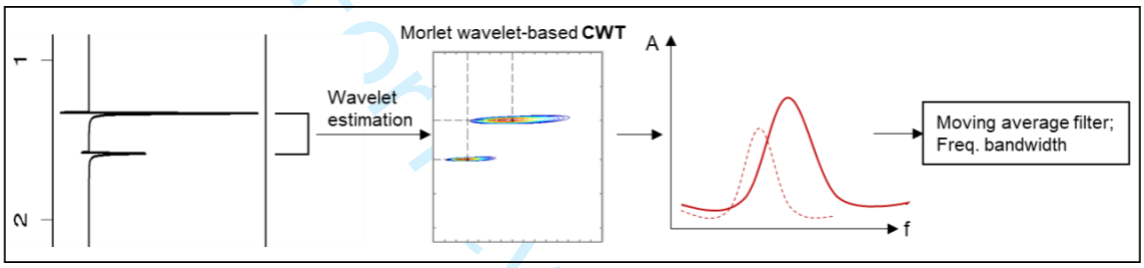

Figure 9. Schematic diagram of technique V.

3. Numerical Example

To investigate the performance of each Q estimation methods and techniques, we implement different combinations of methods and techniques under given conditions. The explored factors are shown in Table 1. One would expect the level of signal frequency to affect the Q estimation due to its frequency dependency. Therefore, we test two candidate frequencies: 50 Hz which approximately accords with traditional seismic reflection surveys, and 1.5 kHz corresponding to high-frequency surveys such as sonic logs. Moreover, noise is another essential factor that would damage the data and Q estimation. Investigation of relations between noise scale and Q estimation has practical significance. Lastly, we test layers of different intrinsic Q values in order to explore measurement accuracy across different geologic media, with the hypothesis being that lower Q values should be measured with greater accuracy due to a more detectable frequency shift. All combinations of parameter values in Table 1 are tested.

Table 1. Cases analyzed

Parameters	Values
Dominant frequency f_p (Hz)	50, 1500
Signal-to-noise ratio S/N (dB)	-1, 5, 10 30, ∞
True model Q	10, 20, 50, 80, 120, 200
Bandwidth coefficient ε	0, 0.1, …, 0.9
Estimation methods	CFS, SRM, PFS
Techniques	TI, TII, TIII, TIV, TV

In order to consider the influence of the "thin-layer" effect and traveltime on Q estimation, we set a wedge model (Figure 10), which is simulated from a Ricker wavelet (Ricker 1953) with frequency of 50 Hz and 1500 Hz and a reflectivity model of which the thickness varies from 0 to 2.5 times of the signal period (T), namely 0 ~ 50 ms for 50 Hz source wavelet and 0 ~ 1.6 ms for 1500 Hz. The reason we set the thickness as units of period is that we hope to discuss the effect of the wavelet overlapping on Q estimation regardless of the velocity. Using period to represent the length of wavelets would account for the situations with different frequencies without the need of considering velocity. The simple 2D synthetic trace data (100 traces) are simulated through convolution of the reflection model with the source wavelets and attenuated reflection

wavelets. The evolution of the amplitude spectrum through time is modeled by

$$R(f) = G(f)H(f)S(f). \quad (9)$$

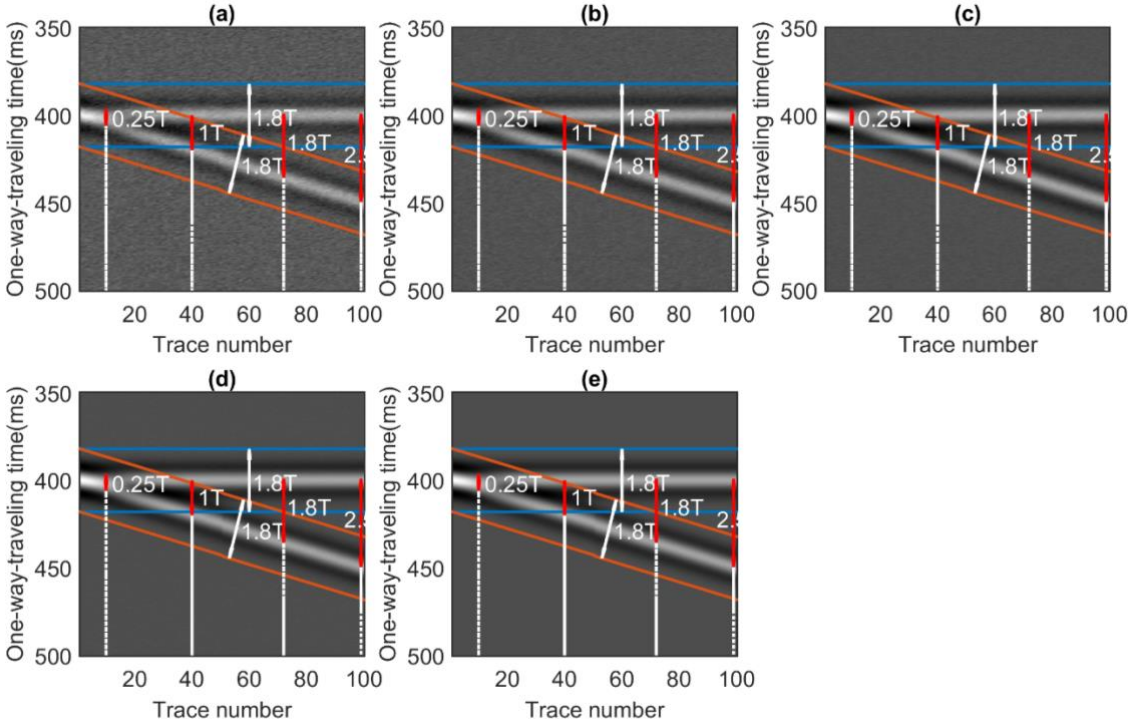

Figure 10. A 2D wedge model used in this study. The minimum thickness is 0 at Trace 1 and the maximum thickness is 2.5 times of the signal period (T) at trace number 100. The S/Ns are (a) -1, (b) 5, (c) 10, (d) 30, (e) ∞, respectively. The solid blue line indicates the picked signal for the first interface, while the red one represents the picked signal for the second interface. The width of each interface is 1.8 times of the signal period. The white dashed lines indicate the trace numbers corresponding to one-way traveltime of 0.25T, 1T, 1.8T, 2.5T, respectively.

Since in the equation 2, 3, 7 there is no term with respect to $G(f)$, including geometric spreading or other factors that do not change with frequency, we can ignore it when forward modeling the seismic wave propagation by convolution, meaning that only the absorption attenuation is considered. Thus, the velocity or density information is not necessary to be assigned to the model because they are not participating in either the absorption calculation or the convolution algorithm. Please note that's different from the wave-equation forward modeling, but effective enough for discussing the Q estimation by those three spectral methods. Also, we only model the zero-offset trace that we can assume the first interface as source wavelets or reference wavelets, which is a very important assumption for those estimation methods. The attenuation is performed in spectral domain for each spectrum by equation 1. For the convenience, all traveltime here is transferred into one-way traveltime. To keep the balance between the temporal resolution and computational cost, we use sample rate dt = 500 μs for the frequency at 50 Hz and dt = 20 μs for the frequency at 1500 Hz. Figure 11 shows the last trace of the wedge model and its spectrum. The five S/Ns -1, 5, 10, 30 and ∞ are investigated.

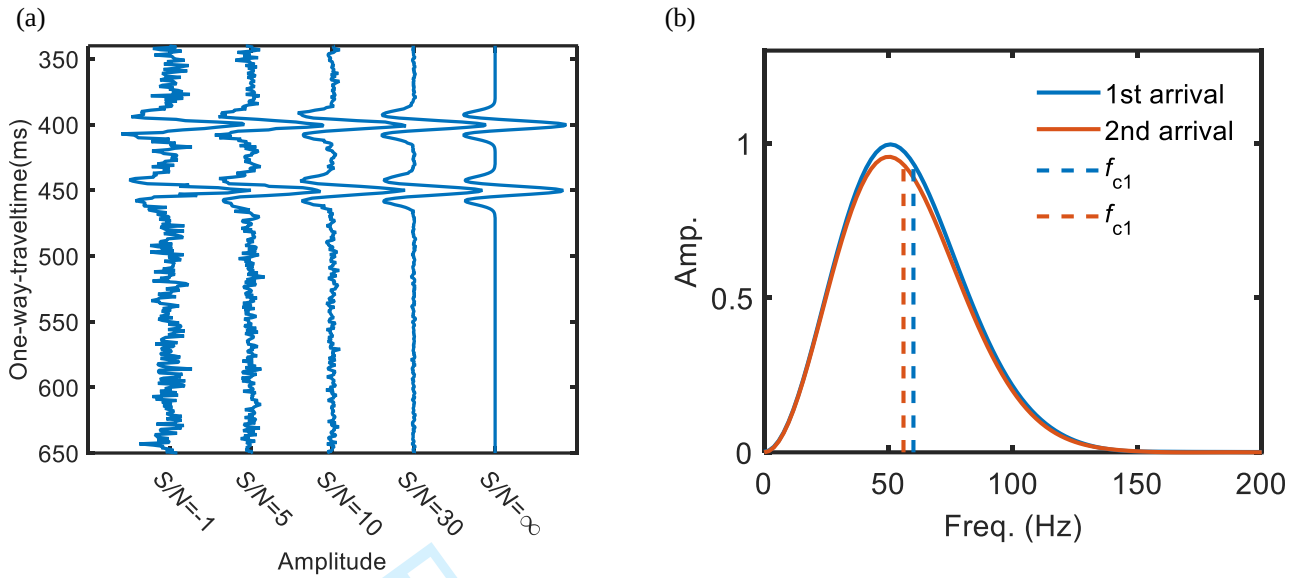

Figure 11. (a) The last trace of wedge model with different S/Ns; (b) the spectrum of first and second arrivals for S/N = ∞ and their centroid frequencies.

4. Results and Discussion

4.1 Window Size Test

Before discussing window size, we must define a mean absolute percentage error (MAPE) to assess the estimation performance. It is the relative error between estimated $\hat{Q}$ and true Q, averaged over the range of traces i, as in equation 10. The "estimation error" in the following discussion means MAPE unless noted otherwise.

$$MAPE(\%) = \frac{1}{N}\sum_{i=1}^{N}\frac{\hat{Q}_i - Q_i}{Q_i} \times 100 \qquad (10)$$

As showed in Figure 10, the window size is defined as the truncated signal length. For instance, the window size of 1.8T (T represents signal period) means to truncate the signal from the 0.9T above the center of the wavelet to 0.9T below the center of the wavelet. The window size determines the effective signal. Too large of a window size will reduce the estimation resolution. Too small of a window size, however, is not able to represent the whole wavelet or leads to frequency leakage when applying Fourier transformation. Before the window size test, we define a concept called "noninterference zone", which represents the traces from which Q is accurately estimated in the wedge model. Figure 12 is a schematic diagram for estimated $\hat{Q}$ varying with different traveltime from 0 to 2.5T. The smaller trace number corresponds to a thinner target layer where there exists a great chance of the wavelet interference. So, in the smaller-trace-number zone, the estimation is not expected to be accurate. While in the noninterference zone the estimated $\hat{Q}$ agrees better with the set-up Q (the absolute percentage error tolerance is set as 5% for this case). The beginning trace of the noninterference zone indicates the minimum traveltime of which the Q is able to be measured under the MAPE of 5%.

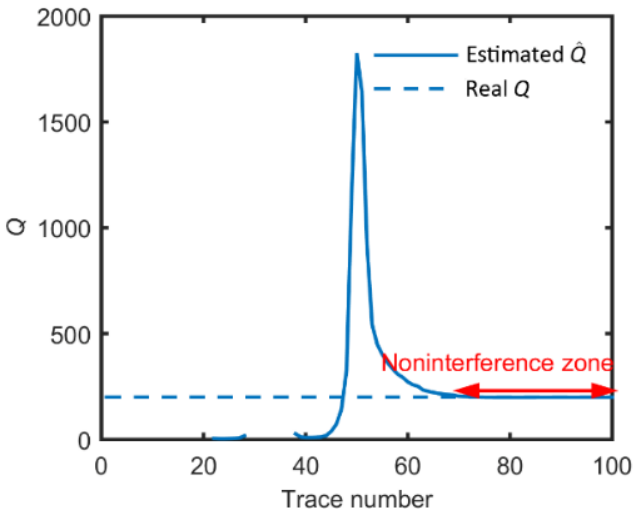

Figure 12. Estimated $\hat{Q}$ from the wedge model varying with different traces. The true Q is set as 200 as the dashed line. The smaller trace number means less traveltime, thus more strong interference of wavelets. The wavelet interference which occurs at trace number less than about 70 between first and second interfaces impairs the Q estimation.

For the purpose of investigation of the optimal window size when conducting Q estimation from reflection data, we implement fifteen combinations of methods and techniques on the model of Q = 200, f_p = 50 Hz, S/N = ∞, with the window size from 0.5T to 2T. In Figure 13(a), it is obvious that the estimation errors reach the minimum when the window size is

larger than 1.5*T*. The larger window size assures the smaller error; however, in Figure 13(b) we can see the noninterference zone starts at a larger trace number (thicker layer) when choosing a bigger window size, which means for larger window size the ability or resolution of the vertical detection decreases. So, there is a trade-off between the estimation error and vertical resolution. Ultimately, we take 1.8*T* as a balanced value for the window size. Conservatively, the trace number 70 could be the beginning of the noninterference zone for all estimations, as these marks where the first and second truncated signals are separated from each other in Figure 10. We also conduct window size tests for models with different *Q*'s and different source wavelets. It leads us to the very similar conclusions.

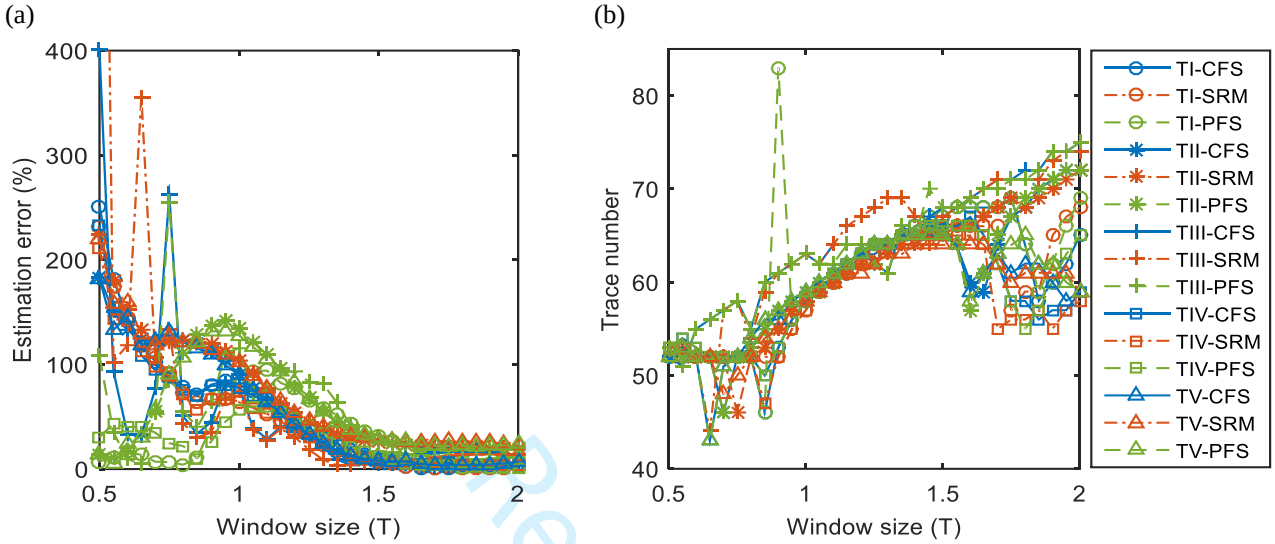

Figure 13. (a) Estimation errors with window size under the condition of f_p = 50 Hz, Q = 200, S/N = ∞; (b) beginning trace of noninterference zone with window size. The larger trace number means the noninterference zone starts at a thicker layer. In other words, larger trace number corresponds to lower vertical estimation resolution.

4.2 Comparison of Methods/Techniques for S/N = ∞ and f_p = 50 Hz

4.2.1 Estimation failure rate/null value occurrence.

Sometimes, the torture of the signal would make the dominant frequency of the received wavelet larger than that of the source wavelet. When this occurs, it produces no estimation of *Q* (null or NA values) or illegitimate estimate of *Q* (i.e., nonpositive values, which we set as null). The estimation failure might occur due to factors such as the interference of noise, spectrum transformation or truncated length. The percentage of the number of the null values to the total trials is defined as the failure rate. Investigation of the failure rate leads us to a view of the ability of the method's or technique's resistance to those factors. We will cover the failure rate in the following discussion.

4.2.2 Influence of the Q model

The true *Q* of the model represents the magnitude of the attenuation. It would be expected to have a better estimation for a highly attenuated model because a larger difference between the source and received wavelets is more detectable with smaller relative error. We analyze the estimation error and failure rate in different perspectives. Figure 14(a) shows the estimation errors with different *Q* models for each technique-method. In general, there is not much relation between the model *Q* and the estimation error. This point could also be demonstrated by the boxplot of MAPEs in Figure 14(b), which counts on data from all technique-methods as a whole. But the smaller model *Q* generates less estimation variance, which makes the *Q* measurement more stable. Additionally, the total estimation failure rate not significantly but gets higher with a larger true *Q* (Figure 15). A possible explanation could be that the smaller *Q* which corresponds to larger attenuation on signal spectrum would diminish the relative errors of frequency shifts (Table 2) when using them as denominator in equation 3 or 7. To sum up here, the accuracy of *Q* estimation by all methods and techniques is subjected to the *Q* model itself.

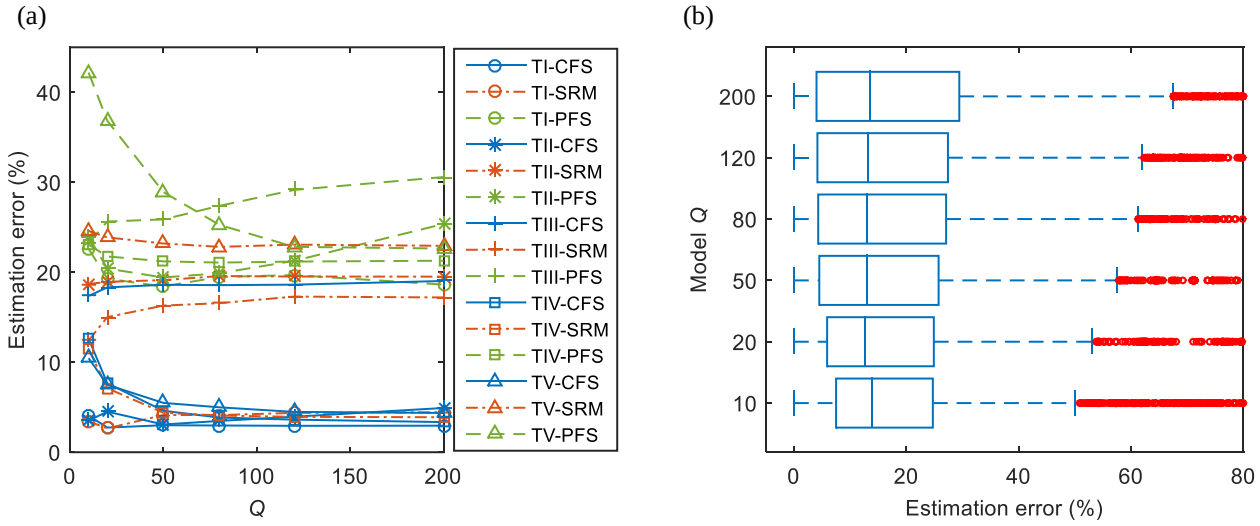

Figure 14. (a) Estimation errors with different Q models; and (b) boxplot of the MAPEs for different Q models under f_p = 50 Hz and S/N = ∞ for the noninterference zone (trace number from 70 to 100). The MAPEs are averaged over all frequency-bandwidth coefficients for the noninterference zone.

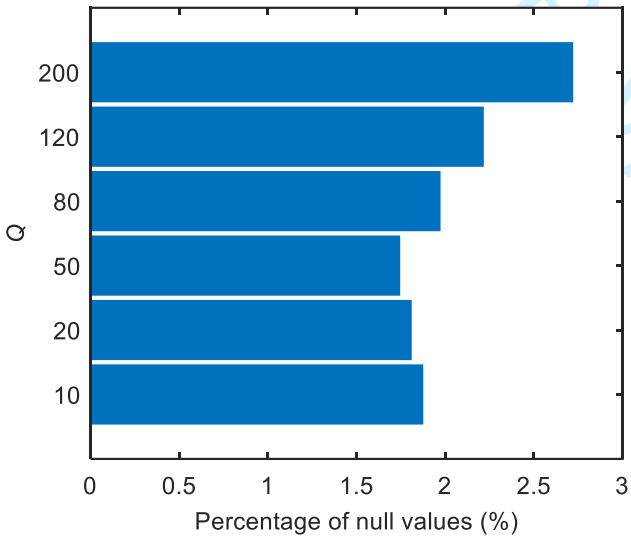

Figure 15. Estimation failure rates of the different Q models averaging traces of all frequency-bandwidth coefficients under f_p = 50 Hz and S/N = ∞ for the noninterference zone (trace number from 70 to 100).

Table 2 Frequency shift (Hz) for different models at different source frequencies.

Model Q		10	20	50	80	120	200
Source freq.	50 Hz	6.81	3.73	2.02	1.80	1.79	1.79
	1500Hz	214.51	111.41	66.25	59.46	59.72	59.93

4.2.3 Influence of the effective frequency bandwidth

The second factor influencing Q estimation is the effective frequency bandwidth. We tested ten effective-bandwidth coefficients 0.0, 0.1, 0.2 …0.9 for all Q models under f_p = 50 Hz and S/N = ∞ (Figure 16). Different from last analysis, the estimation errors are averaged over all Q models, not bandwidth coefficients. We still merely take the noninterference zone, trace 70 to 100, into consideration. Figure 17(a) and Figure 17(b) count data from all technique-methods on. From Figure 17(a), bandwidth coefficients in the range of [~0.2, ~0.4] show consistently low errors for all techniques and methods with less failure rates (Figure 17(b)). In other words, the effective frequency bandwidth which covers about 60%~70% of the received wave spectrum successfully eliminates the noise or other calculation errors within very low and very high frequencies (equation 8). The analysis offers us a proper choice of the bandwidth coefficient.

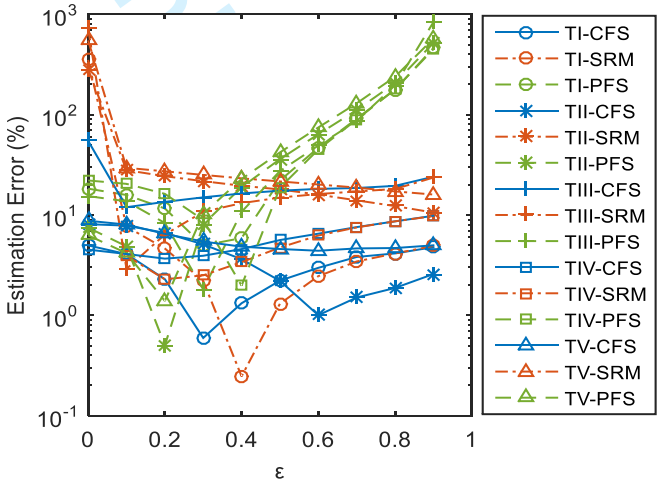

Figure 16. Estimation errors with different bandwidth coefficients under f_p = 50 Hz and S/N = ∞. The MAPEs are averaged over all Q models for the noninterference zone (trace number from 70 to 100).

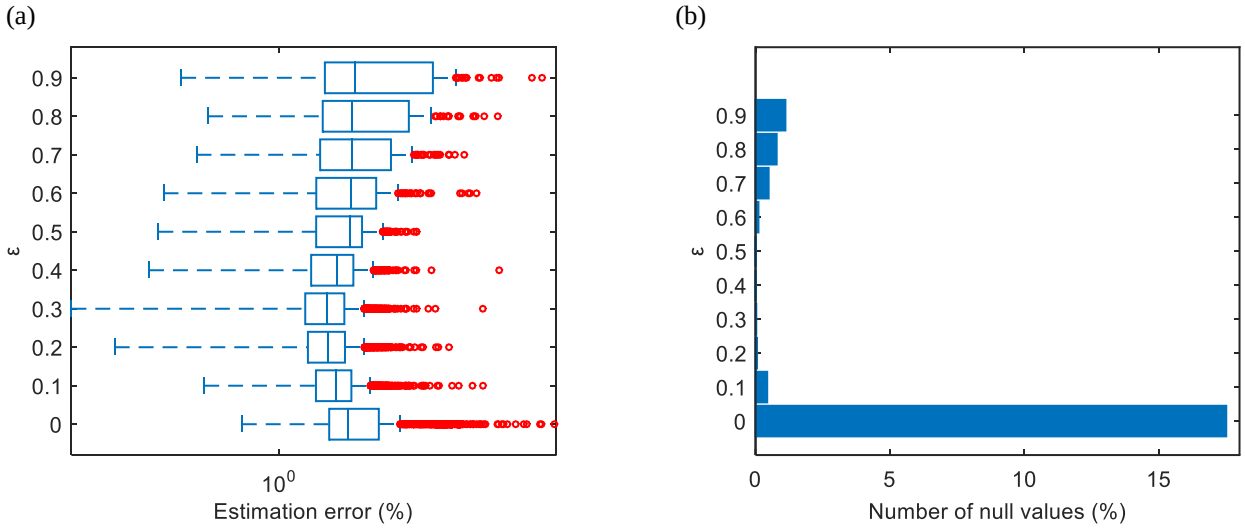

Figure 17. (a) Estimation failure rates of the different bandwidth coefficients averaging all Q models; and (b) boxplot of the MAPEs for different bandwidth coefficients under f_p = 50 Hz and S/N = ∞. The MAPEs are averaged over all Q models for the noninterference zone (trace number from 70 to 100).

4.2.4 Optimal methods/techniques

Figure 18, 19, and 20 show the performance of fifteen combinations of techniques and methods. They consider the data from all Q models and bandwidth coefficients. In Figure 18, the estimation error of CFS is consistently much lower than other methods, even though for technique III and IV errors of CFS and SRM are very close. Technique I and IV performs better than other techniques, especially for CFS and SRM. And their failure rates stay at low levels (Figure 19(b)). Figure 19(a) shows the combination of Technique I and CFS has lowest estimation error.

The reason that technique III has larger error rates is that implementing an estimated-wavelet-based CWT would add the wavelet-extraction error to the frequency transformation. On the other hand, the demanded spectrum after conducting CWT on the windowed signal is just a slice of the time-frequency map. It only considers one instantaneous time, thus more sensitive to errors. Even using average of the spectrum, it would lead to bias to the instantaneous reflection time. In addition, the mother wavelet is supposed to satisfy a technical condition of behaving like a wave (Aguiar-Conraria and Soares 2011), which is difficult to assure in wavelet estimation. On the contrary, the technique I and IV, for example, applying FFT which takes all time window has less error rate. In terms of the worse performance of PFS, this method relies on the accuracy of peak frequency extraction, which is sensitive to errors and difficult to precisely obtain in practice.

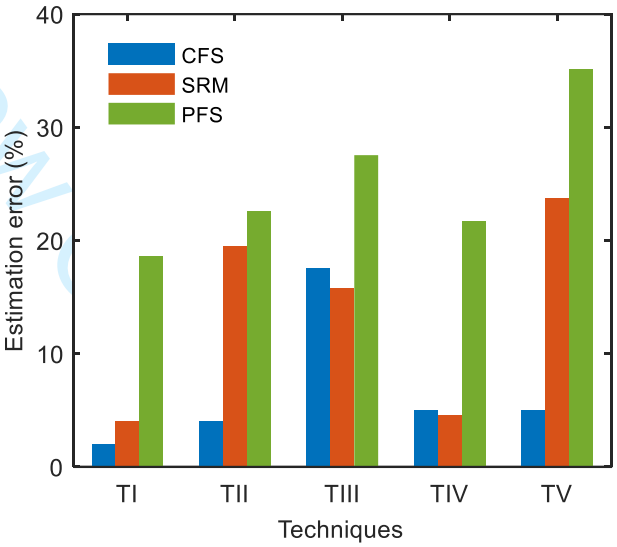

Figure 18. Estimation errors for methods/techniques averaging over all Q models and bandwidth coefficients for the noninterference zone (trace number from 70 to 100).

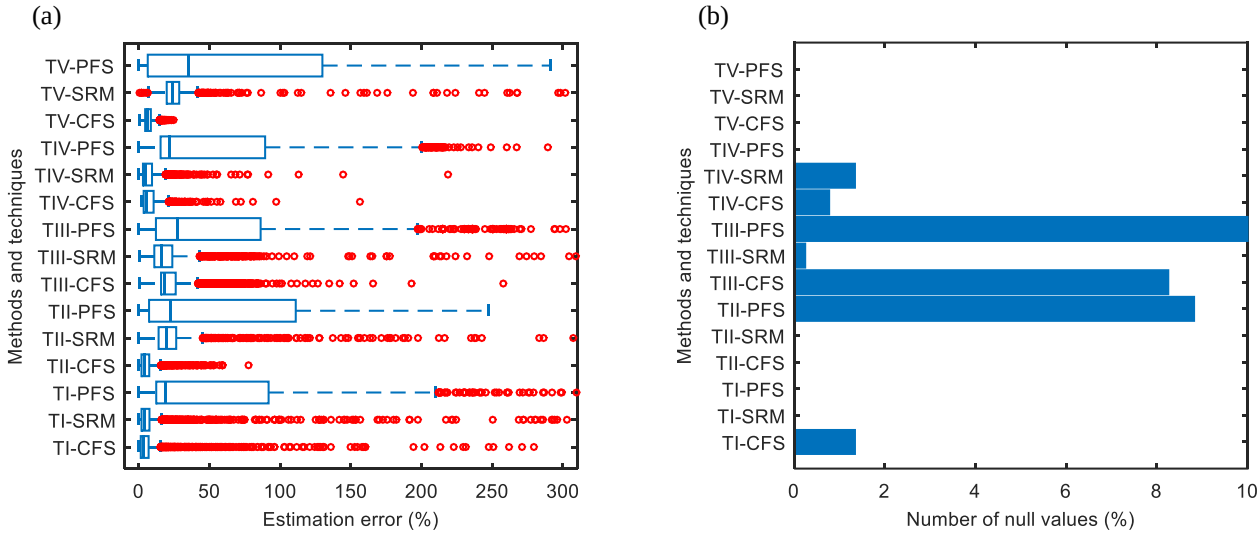

Figure 19. (a) Boxplot of the MAPEs for methods/techniques; (b) estimation failure rates of methods/techniques averaging all Q models and bandwidth coefficients. Both are condition of $f_p = 50$ Hz and S/N = ∞ for the noninterference zone (trace number from 70 to 100).

4.3 S/N Analysis for f_p = 50 Hz

As one would expect, the error rate generally increases with larger amounts of noise or smaller S/N. Figure 20(a) shows CFS stays at the lowest level of errors except for pairing with Technique III, even across S/N levels. We can also see that TI and TIV perform the best among five techniques except for pairing with PFS in both Figure 20(a) and Figure 22. And Figure 21 proves the hypothesis that the larger magnitude of noise harms the Q estimation in both estimation errors and failure rates. As expected, Figure 20(b) shows that null values occur with greater frequency as more noise is added to the signal, and technique I and IV have low failure rates. Summarily, we could reach the conclusion that techniques I or IV paired with methods CFS or SRM are the optimal choices when conducting Q estimation under different levels of noise (Figure 20(b) and Figure 22).

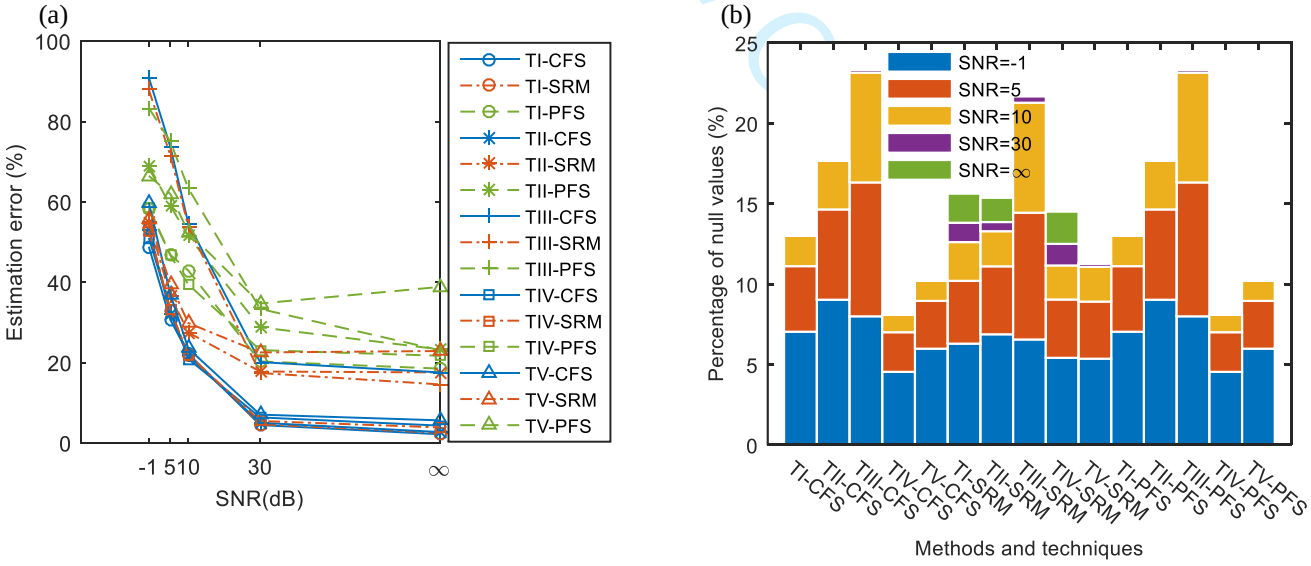

Figure 20. (a) Estimation errors with different S/Ns under f_p = 50 Hz. The MAPEs are averaged over all Q models and bandwidth coefficients for the noninterference zone (trace number from 70 to 100); (b) estimation failure rates for different methods and techniques with different S/Ns under f_p = 50 Hz. The percentages of null values are averaged over all Q models and bandwidth coefficients for the noninterference zone.

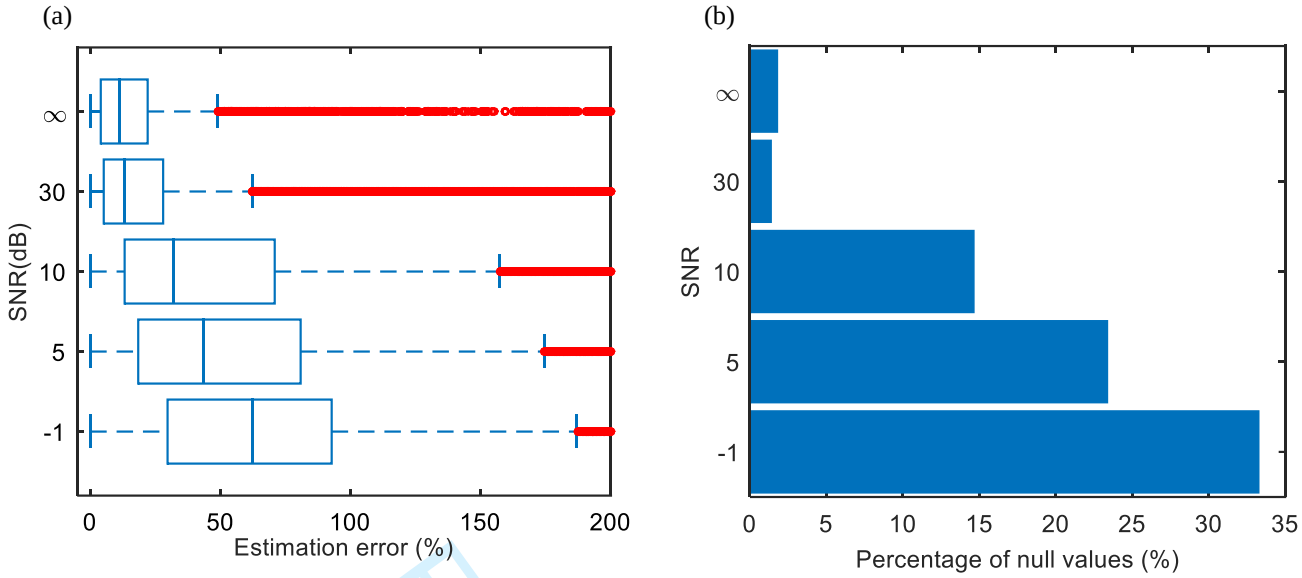

Figure 21. (a) Boxplot of the MAPEs under f_p = 50 Hz for the noninterference zone (trace number from 70 to 100); (b) estimation failure rates with different S/Ns. The percentages of null values are averaged over all Q models and bandwidth coefficients for the noninterference zone.

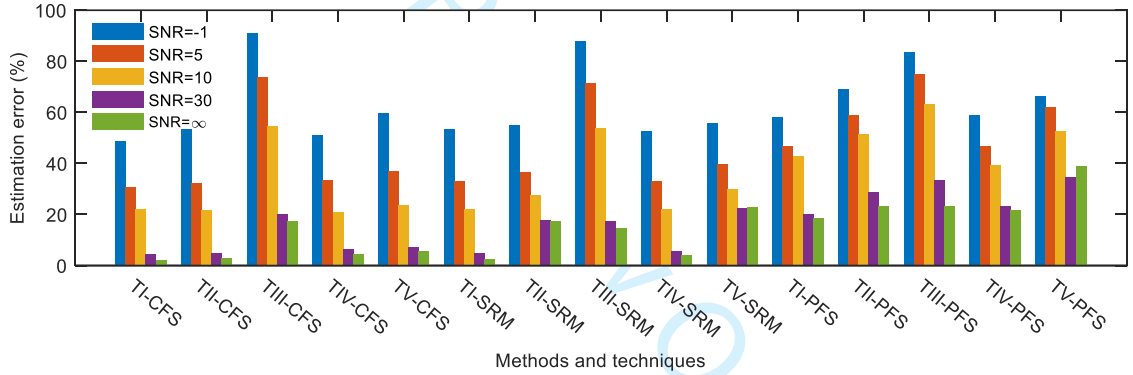

Figure 22. Estimation errors for methods/techniques averaging over all Q models and bandwidth coefficients for the noninterference zone (trace number from 70 to 100, f_p = 50 Hz).

4.4 High Frequency Case (f_p = 1500 Hz)

From Figure 23(a) to Figure 25, it is easy to reach the same conclusion even though we carry out estimation under different frequencies; however, the MAPEs are much smaller than that of 50 Hz case comparing Figure 25 with Figure 22. Because the relative error resulting from the absolute frequency shift decreases (Table 2) while coping with a higher frequency signal. Meanwhile, we have less estimation failure according to Figure 23(b) and Figure 24(b). So, the high-frequency case is easier to measure accurate Q.

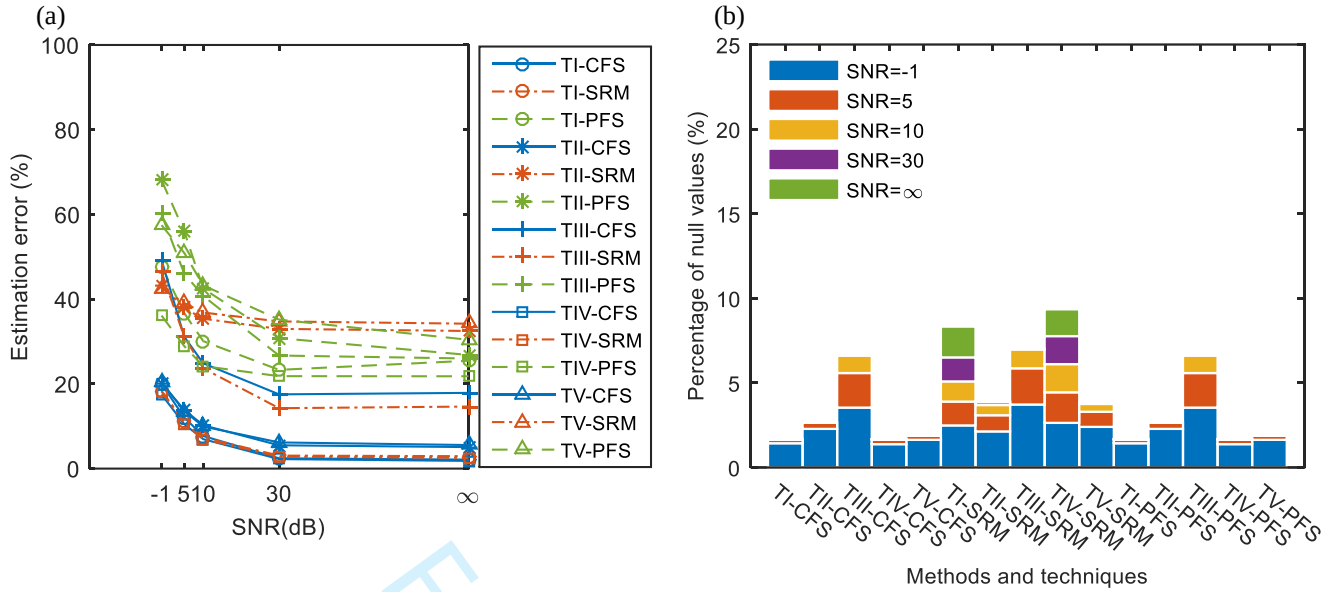

Figure 23. (a) Estimation errors with different S/Ns under f_p = 1500 Hz. The MAPEs are averaged over all Q models and bandwidth coefficients for the noninterference zone (trace number from 70 to 100); (b) estimation failure rates for different methods and techniques with different S/Ns under f_p = 1500 Hz. The percentages of null values are averaged over all Q models and bandwidth coefficients for the noninterference zone.

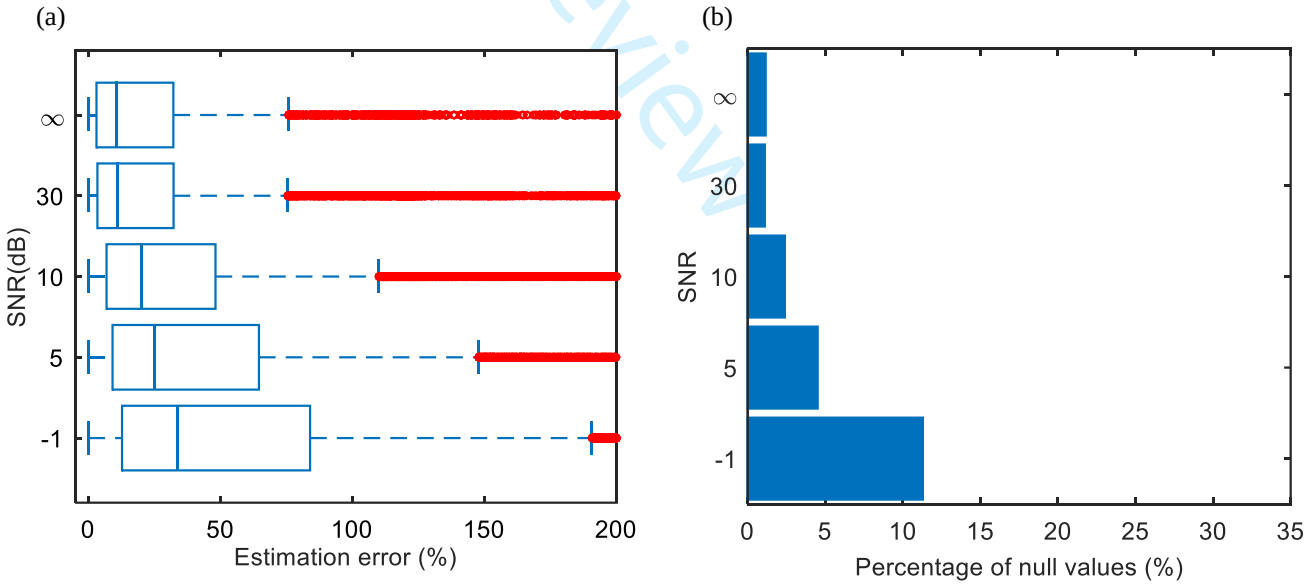

Figure 24. (a) Boxplot of the MAPEs under f_p = 1500 Hz for the noninterference zone (trace number from 70 to 100); (b) estimation failure rates with different. The percentages of null values are averaged over all Q models and bandwidth coefficients for the noninterference zone.

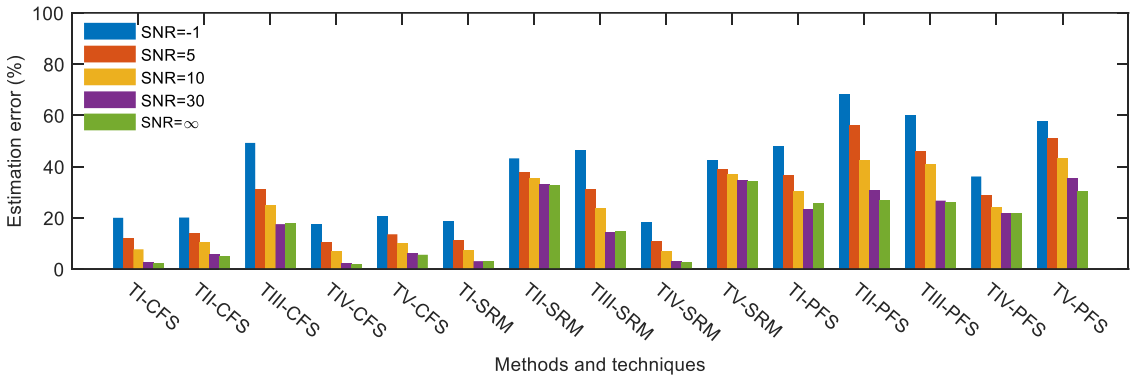

Figure 25. Estimation errors for methods/techniques averaging over all Q models and bandwidth coefficients for the noninterference zone (trace number from 70 to 100, f_p = 1500 Hz).

4.5 "Thin-layer" Effect

As discussed in Figure 12, when it comes to a very thin layer (trace number less than 70 or one-way traveltime less than 1.8T), the source and reflection wavelets interfere with each other, which will torture the signal spectra, leading to estimation failure or bias. Lu *et al* (2007) proposed a high-order statics method to restore the wavelet, which is carried out on Technique IV and V. One would expect technique IV and V give less error rates than others for trace number less than 70 which is in the interference zone. We analyze the estimation errors and failure rates for trace number from 60 to 65. Figure 26(a) and Figure 27 demonstrate the hypothesis that the wavelet extraction improves the performance of Q measurements. Moreover, TIV and TV has less failure rates than other techniques (Figure 26(b), Figure 27). This experiment tells us the wavelet estimation benefits the Q estimation in this aspect, even though it increases the error when associated with CWT.

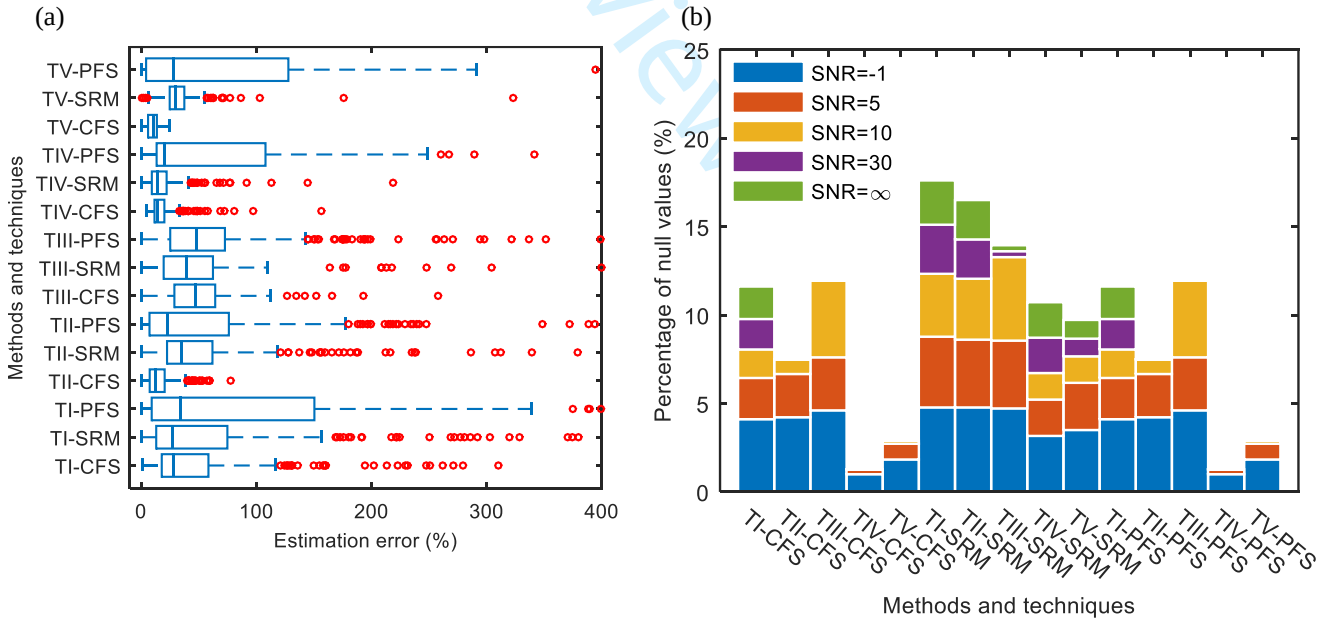

Figure 26. (a) Boxplot of the MAPEs for methods/techniques under f_p = 50 Hz and S/N = ∞ for the interference zone (trace number from 60 to 65); (b) estimation failure rates for different methods and techniques under f_p = 50 Hz. The percentages of null values are averaged over all Q models and bandwidth coefficients for the interference zone.

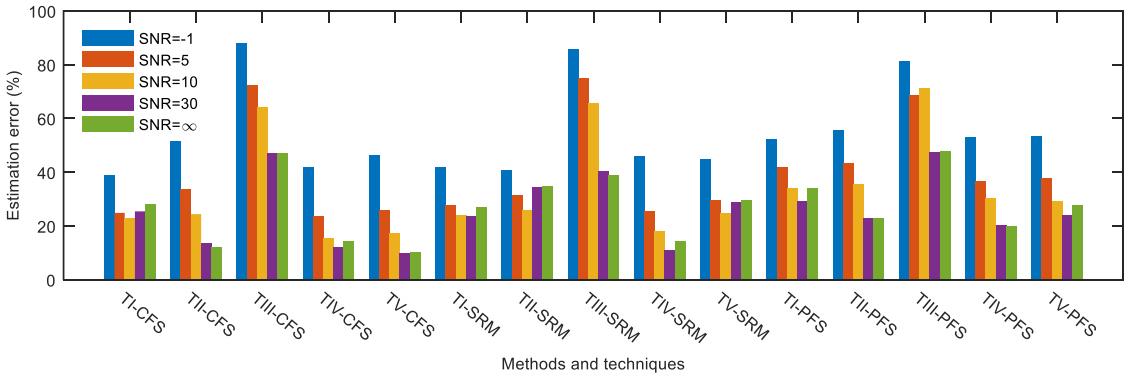

Figure 27. Estimation error for methods/techniques averaging over all Q models and bandwidth coefficients for the interference zone (trace number from 60 to 65, f_p = 50 Hz).

5. Conclusion

Three main Q estimation approaches, CFS, SRM and PFS, have been specifically analyzed. Regardless of the scattering or other frequency-independent factors in Q estimation, accurate Q measurement from seismic reflection data, especially for prestack data, is still difficult because of much more noise intervention and more difficult interface tracking. Data preprocessing is necessary to obtain a reliable Q. Through this research, we provide a detailed procedure including best options to preprocess data and the optimal parameter choice under difference conditions for Q estimation especially when dealing with reflected seismic data.

Although the analysis in this research is based on simulated data (actually, the real Q in practical data is hard to know), we consider a complete set of conditions that might be faced in practice. The conclusions made here are significant in guiding the practical application. For three frequency-domain methods, five kinds of preprocessing procedures are implemented on synthetic data before Q estimation. After analyzing six models with ten bandwidth coefficients: firstly, the best window size when truncating signals as the source or received wavelet is 1.8 times of the signal period. This is a trade-off value considering both the estimation error and temporal estimation resolution. Secondly, even though it is not significant, Q of the greatly attenuated cases can be more accurately estimated because of the relative error decreasing. Additionally, the effective frequency bandwidth choice is essential to all estimation methods because the noise interference in very low or high bandwidth would have a large effect on the frequency shift. Generally, the effective-bandwidth coefficient within 0.2 ~ 0.4 is a good value. Moreover, any pair of technique I or IV and CFS or SRM gives us a smaller MAPE which could be the optimal choice of methods and techniques. And as expected, the Q estimation needs signals with lower levels of noise. The combinations of technique I or IV and CFS or SRM still perform better than others in cases with even higher levels of noise. But we could see that technique IV is superior in some cases because of its stronger capability of wavelet restoring once in practice where there is a "thin layer" effect, even though it brings more errors from the wavelet estimation. Lastly, carrying out tests on a higher frequency condition, the MAPE decreases for each scenario. This is good news for Q estimation from high-resolution, near-surface surveys which usually have higher frequencies.

So far, we specifically suggest the Q estimation method and their preprocessing techniques in order to have a better Q measurement. But there is still a problem that we do not cover, namely, the source frequency which is required to know in advance in those three methods. What we can do now in practice is to pick up the first arrival as an approximation for the source wavelet. Maybe more advanced theory should be proposed to overcome the difficulty in acquiring source wavelet in practice.

References

Aguiar-Conraria L and Soares M J 2011 The Continuous Wavelet Transform: A Primer *Nipe Wp* 6–8

Bath M 1974 Spectral Analysis in Geophysics *Developments in Solid Earth Geophysics* 7 563

Blias E 2011 Q-factor estimation through optimization approach to near-offset VSP data *SEG Technical Program Expanded Abstracts 2011* 4278–4282

Cheng P and Margrave G F 2013 Estimation of Q : a comparison of different computational methods *CSPG/CSEG/CWLS GeoConvention* 12 2–5

Dasgupta R and Clark R A 1998 Estimation of Q from surface seismic reflection data *Geophysics* 63 2120

Dutta G and Schuster G T 2016 Wave-equation Q tomography *GEOPHYSICS* Society of Exploration Geophysicists 81 R471–R484

Engelhard L 1996 Determination of Seismic-Wave Attenuation By Complex Trace Analysis *Geophysical Journal International* 125 608–622

Frisillo A L and Stewart T J 1980 Effect of partial gas/brine saturation on ultrasonic absorption in sandstone *Journal of Geophysical Research* 85 5209

Gao J, Li Y, and Chen W 1998 On the instantaneous attributes analysis of seismic data via wavelet transform *68th Ann. Internat. Mtg* 1084–1087

Gladwin M T and Stacey F D 1974 Anelastic Degradation of Acoustic Pulses in Rock *Physics of the Earth and Planetary Interiors* 8 332–336

Goutbeek F H, Dost B, and van Eck T 2004 Intrinsic absorption and scattering attenuation in the southern part of the Netherlands *Journal of Seismology* 8 11–23

Hackert C L and Parra J O 2004 Improving Q estimates from seismic reflection data using well-log-based localized spectral correction *Geophysics* Society of Exploration Geophysicists 69 1521

Harris F J 1978 On the use of windows for harmonic analysis with the discrete Fourier transform *Proceedings of the IEEE* 66 51–83

Hatzidimitriou P M 1994 Scattering and anelastic attenuation of seismic energy in northern Greece *pure and applied geophysics* 143 587–601

Hauge P S 1981 Measurements of attenuation from vertical seismic profiles *Geophysics* 46 1548–1558

Jannsen D, Voss J, and Theilen F 1985 Comparison of methods to determine Q in shallow marine sediments from vertical reflection seismograms *Geophysical Prospecting* 479–497

Karl J H 1989 8 - Digital Filter Design in *Introduction to Digital Signal Processing* ed. J. H. Karl San Diego: Academic Press pp. 165–196

Kjartansson E 1979 Constant Q-Wave Propagation and Attenuation *Journal of Geophysical Researchch* 84 4737–4748

Lu W, Zhang Y, Zhang S, and Xiao H 2007 Blind wavelet estimation using a zero-lag slice of the fourth-order statistics *Journal of Geophysics and Engineering* IOP Publishing 4 24–30

Müller T M, Gurevich B, and Lebedev M 2010 Seismic wave attenuation and dispersion resulting from wave-induced flow in porous rocks — A review *Geophysics* 75 75A147

Neep J P, Sams M S, Worthington M H, and O'Hara-Dhand K A 1996 Measurement of seismic attenuation from high-resolution crosshole data *Geophysics* 61 1175–1188

Oliveira F de S, de Figueiredo J J S, Oliveira A G, Schleicher J, and Araújo I C S 2017 Estimation of quality factor based on peak frequency-shift method and redatuming operator: Application in real data set *GEOPHYSICS* Society of Exploration Geophysicists 82 N1–N12

Pinson L J W W, Henstock T J, Dix J K, and Bull J M 2008 Estimating quality factor and mean grain size of sediments from high-resolution marine seismic data *Geophysics* 73 G19–G28

Quan Y and Harris M J 1997 Seismic attenuation tomography using the frequency shift method *Geophysics* 62 895

Raikes S A and White R E 1984 Measurements of Earth Attenuation from Downhole and Surface Seismic Recordings *Geophysical Prospecting* 32 892–919

Ricker N 1953 THE FORM AND LAWS OF PROPAGATION OF SEISMIC WAVELETS *GEOPHYSICS* Society of Exploration Geophysicists 18 10–40

Rickett J 2006 Integrated estimation of interval-attenuation profiles *GEOPHYSICS* Society of Exploration Geophysicists 71 A19–A23

Rossi G, Gei D, Böhm G, Madrussani G, and Carcione J M 2007 Attenuation tomography: An application to gas hydrate and free gas detection *Geophysical Prospecting* 55 655–669

Sams M and Goldberg D 1990 The validity of Q estimates from borehole data using spectral ratios *GEOPHYSICS* Society of Exploration Geophysicists 55 97–101

Sheriff R E and Geldart L P 1995 *Exploration Seismology* Cambridge University Press

Tary J B, van der Baan M, and Herrera R H 2017 Applications of high-resolution time-frequency transforms to attenuation estimation *GEOPHYSICS* Society of Exploration Geophysicists 82 V7–V20

Toksöz M N, Johnston D H, and Timur A 1979 Attenuation of seismic waves in dry and saturated rocks: II. Mechanisms *Geophysics* 44 691

Tonn R 1991 the Determination O F the Seismic Quality Factor Q From Vsp Data: a Comparison of Different Computational Methods' R a I N E R T O N N 2 *Geophysical Prospecting* 39

Tu N and Lu W 2010 Improve Q estimates with spectrum correction based on seismic wavelet estimation *Applied Geophysics* 7 217–228

Winkler K W and Nur A 1982 Seismic attenuation: effects of pore fluids and frictional sliding *Geophysics* 47

Zhang C and Ulrych T J 2002 Estimation of quality factors from CMP records *Geophysics* 67 1542

Zhang R-W, Li H-Q, Wen P-F, and Zhang B-J 2016 THE VELOCITY DISPERSION AND ATTENUATION OF MARINE HYDRATE-BEARING SEDIMENTS *Chinese Journal of Geophysics* 59 539–550